Title: Phosphorus stress and spatial confinement lower the threshold for quorum-sensing activation of redox-active metabolite production in *Pseudomonas synxantha*

Authors: R. E. Alcalde[1], H. Jeckel[1], O. Zhang[2], R. L. Avila[1], N. Dalleska[3], D. Mavrodi[4], C. Yang[5], D. K. Newman[1,6,a]

[1]Division of Biology and Biological Engineering, California Institute of Technology, Pasadena, CA 91125

[2]Department of Physics & Astronomy, Texas A&M University, College Station, TX 77843

[3]Global Environmental Center, California Institute of Technology, Pasadena, CA 91125

[4]USDA, Agricultural Research Service, Wheat Health, Genetics and Quality Research Unit, Pullman, Washington, USA

[5]Division of Engineering and Applied Science, California Institute of Technology, Pasadena, CA 91125

[6]Division of Geological and Planetary Sciences, California Institute of Technology, Pasadena, CA 91125

[a]To whom correspondence may be addressed. Email: dkn@caltech.edu

Abstract:

Bacteria often coordinate collective behaviors such as biofilm formation and secondary metabolite production through quorum sensing (QS), a regulatory system traditionally linked to high cell density. However, in environments like soil, where microbial populations are spatially fragmented, sparse, nutrient-limited, and subject to mass transport, the mechanisms that enable QS-dependent processes remain incompletely understood. Here, we investigate the regulation of a secreted redox-active metabolite, phenazine-1-carboxylic acid (PCA), in *Pseudomonas synxantha* 2-79, a model rhizobacterium, under phosphorus (P) limitation, a persistent stress in many soils. Using a combination of microscopy and molecular genetic approaches, we show that P limitation sensitizes the QS activation threshold by an order of magnitude, enabling phenazine induction at relatively low population densities in

comparison to P replete conditions. This induction is abolished in QS-deficient mutants and restored by the addition of exogenous acyl-homoserine lactone (AHL), demonstrating that quorum sensing remains essential but its threshold becomes environmentally tuned. Under P limitation, spatial confinement and pore saturation levels further shape the timing and location of induction, illustrating how physical structure and nutrient stress can modulate bacterial activities. Moreover, phosphorus stress confers both collaborative and competitive advantages, enabling *P. synxantha* to undergo low-cell density AHL cross-talk between related *Pseudomonas* spp. and to suppress other rhizobacteria. Lastly, on plant roots, PCA genes were more predominantly induced under P limitation. These findings illustrate how the nutrient status of an environment can modulate the onset of quorum sensing, enabling quorum-regulated behaviors to activate at lower thresholds.

Introduction:

Soil microbes sustain ecosystems. Through their metabolism, they drive nutrient cycling, modulate plant health, and influence mineral weathering. Many of these functions depend not only on individual physiology but on the coordinated activity of microbial populations and communities, often mediated through the release of small molecules that act as public goods, chemical signals, or antibiotics. Among these, phenazines—redox-active metabolites produced by diverse soil bacteria that support a variety of biological functions[1–4]—are particularly notable. Through their redox chemistry, they promote phosphorus[5,6] and iron availability,[7–10] shape microbial competition,[11–13] and affect plant-microbe interactions[14–16] in the rhizosphere.

Phenazine biosynthesis is typically controlled by quorum sensing (QS), a gene regulatory system in which bacteria produce and respond to diffusible signals, such as acyl-homoserine lactones (AHLs), to coordinate group-level behaviors.[17,18] Once a threshold concentration of signal accumulates, often reflected by high cell density, QS activates gene expression for costly cooperative functions like biofilm formation, virulence, or secondary metabolite production.[19–25] This framework is well supported in

48 laboratory systems. However, in natural environments like soil, microbial populations are often spatially
49 fragmented, sparse, and physically confined within pore structures,[26–28] conditions that can shift signal
50 accumulation and QS activation. Cluster analyses in structured soils report that larger clusters (>100 cells)
51 become sparse as water content decreases, implying many neighborhoods fall below 100 cells.[26] Despite
52 this, phenazines[29,30,4], and other QS-regulated metabolites[31–33] are commonly detected in the rhizosphere.
53 How, then, are these behaviors triggered in environments where signal accumulation may be restricted?

54 Several models emphasize that QS dynamics also depend on environmental structure and signal transport.
55 Diffusion sensing and efficiency sensing—alternative descriptions of quorum sensing— describe how
56 mass transfer, spatial confinement, and local cell organization determine whether signal concentrations
57 reach activation thresholds.[34–37] In structured habitats like biofilms and soils, spatial confinement and
58 mass transfer limitation may allow signals to accumulate locally even when bulk population density is
59 low.[28,38–41] Consistent with this view, a few single cells confined in picoliter microfluidic chambers
60 initiate "high-density" QS programs.[38] Likewise, flow cell experiments show that advection suppresses
61 QS in exposed regions of a biofilm while sheltered niches maintain activation.[42]

62 Beyond physical structure and transport, rhizosphere chemistry and biology, such as nutrient limitation,
63 physicochemical stress, and host-derived cues can also tune QS induction[43]. Here we focus on
64 phosphorus limitation in *Pseudomonas synxantha* (formerly *P. fluorescens*) 2-79, a plant growth-
65 promoting rhizobacterium that produces phenazine-1-carboxylic acid (PCA).[44,45] In this strain, PCA
66 production is governed by a single AHL-based quorum-sensing system, PhzIR; deletion of either *phzI* or
67 *phzR* abolishes PCA production.[45–47] Although PCA increases under phosphate limitation,[6,48] whether this
68 induction is mediated by the PhzIR circuit, arises via cross-talk with other QS pathways, or is driven
69 independently of QS remains unknown. This organism-level question is motivated by the broader soil
70 context: freely available inorganic phosphate is extremely low because much of it is immobilized through
71 sorption to mineral surfaces, [49–51] and in *Pseudomonas aeruginosa*, phosphate (and iron) limitation is

72 known to influence secondary metabolism through multiple QS pathways (e.g., PQS, IQS, RhlR)[52–58] via
73 the PhoBR two component system central phosphate sensing and response.[59–61]

74 We set out to determine whether phosphate stress alters QS dynamics in *P. synxantha* 2-79. Specifically,
75 whether phosphate-limited induction of PCA is QS-dependent or QS-independent. We postulated that
76 phosphate stress would trigger AHL-based PhzIR circuits, thereby lowering the effective QS cell density
77 threshold because PCA production under P limitation occurs at lower cell densities in comparison to
78 standard conditions.[48] We further hypothesized that structured environments act with phosphate levels to
79 shape the onset, location, and ecological consequences of QS-regulated behaviors. To test these
80 predictions, we integrated genetic, optical, and ecological approaches to better understand the rules
81 governing microbial coordination in nature.

82 **Results**

83 **Phosphorus limited environments enhance phenazine gene expression of *Pseudomonas synxantha* in**
84 **plant root microcosms**

85 To begin exploring how phenazine biosynthesis responds to phosphorus availability in the rhizosphere,
86 we imaged *Pseudomonas synxantha* 2-79 colonizing *Brachypodium distachyon* Bd21-3 roots under
87 phosphorus-replete (P-rep; excess inorganic phosphate in medium), phosphorus-limited (P-lim; no
88 inorganic phosphate in medium), and phosphate-sequestering (P-HFO; phosphate bound to iron, i.e., not
89 bioavailable) conditions using light sheet fluorescence microscopy (LSFM). In many Fe-oxide–rich,
90 acidic to neutral soils, phosphate is strongly retained by iron oxides (e.g., hydrous ferric oxide
91 (HFO)),[50,62,63] so our P–HFO treatment approximated this sequestration. A dual fluorescent reporter was
92 used to track phenazine biosynthesis gene expression (P_{phzA}-GFP, green channel) and colonization density
93 proxy (constitutive, P_{tac}-mCherry, red channel). Fluorescence intensity was quantified from maximum
94 intensity projections (MIPs) of LSFM images. For each object within a region of interest the mean

95 intensity was calculated as integrated density divided by object area. This metric approximates
96 fluorescence per unit area in 2D projections, serving as a proxy for relative reporter expression and cell
97 density in colonized regions. Bar plots and Empirical Cumulative Distribution Functions (ECDFs)
98 revealed condition-specific differences in both fluorescence magnitude and distribution (Fig. 1A–B).

99 Induction of phenazine biosynthesis (P_{phzA};) was highest under the P-HFO condition (mean = 0.138),
100 followed by P-lim (mean = 0.061), while remaining minimal under P-replete conditions (mean = 0.016).
101 Although the P-lim condition exhibited lower average expression than P-HFO, its distribution was
102 markedly right-skewed and heavy-tailed, indicating rare but strong induction events. In contrast, P-HFO
103 displayed a broader, moderate distribution, while P-rep remained narrowly distributed around low
104 fluorescence values (Fig. 1B). Representative LSFM images corroborated these findings, revealing robust
105 activation of the P_{phzA} reporter under P-HFO but not under P-replete conditions (Fig. 1C). Interestingly,
106 phenazine expression did not directly correlate with cell density. The constitutive reporter was highest in
107 P-HFO and P-rep (means = 0.117 and 0.115, respectively) and lower under P-lim (mean = 0.051), yet
108 only P-lim and P-HFO conditions induced the phenazine reporter.

109 These observations indicate that at the time of measurement, the cell density was insufficient to trigger
110 phenazine gene expression under nutrient-replete conditions. How, then, does phosphorus limitation
111 stimulate phenazine gene induction at local colonization levels that fail to trigger expression under
112 phosphorus-replete conditions? This observation suggests that canonical QS induction of phenazines may
113 be altered under nutrient stress, but whether this results from a bypass of QS regulation, an increased
114 sensitivity to quorum signals, or integration with parallel stress-response pathways was unclear. We set
115 out to disentangle these possibilities.

116

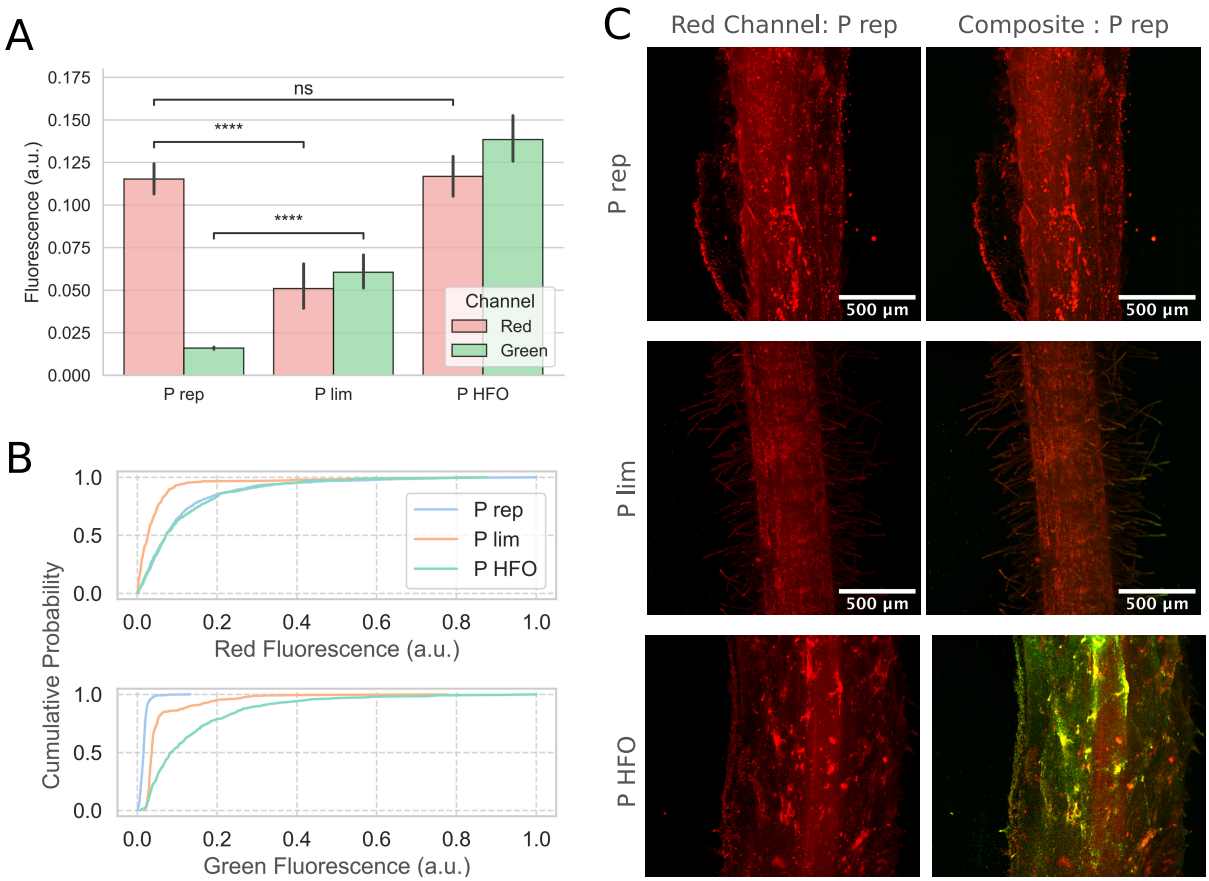

Figure 1: Phenazine gene expression of *Pseudomonas synxantha* 2-79 on plant roots under different phosphorus conditions. (A) Bar plots showing mean ± 95% of normalized red channel (constitutive; P_{tac}) and green channel (phenazine biosynthesis; P_{phzA}) fluorescence intensities under phosphorus-replete (P-rep), phosphorus-limited (P-lim), and phosphate-sorbing hydrous ferric oxide (P-HFO) conditions. Statistical comparisons were performed using two-sided Mann–Whitney tests; significance is indicated by asterisks (ns, not significant; **** $p < 0.0001$). **(B)** Empirical cumulative distribution functions (ECDFs) of normalized fluorescence intensities from the same dataset shown in (A), illustrating the distribution of object-level fluorescence values across experimental conditions. **(C)** Representative maximum intensity projection (MIP) images acquired by light sheet fluorescence microscopy (LSFM) of *P. synxantha* colonizing plant roots under P-rep, P-lim and P-HFO conditions. Red channel images (left) are shown with identical intensity thresholds to compare red fluorescence. Composite images (right) overlay red and green channels using the same fixed thresholds across conditions, revealing differences in P_{phzA} reporter induction. Scale bars = 500 µm. See also Movie S1 for a 3D reconstruction, Table S1 for summary statistics, and Figure S1 for object-level strip plot.

Quorum sensing is required for phenazine production under phosphorus limitation, and phosphate stress sensitizes the QS system to AHL.

134 To determine whether phenazine production under phosphorus limitation requires the *phzIR* quorum
135 sensing (QS) pathway, we examined wild type and mutants defective in either the phenazine production
136 genes (*phzA*-*G*), the QS signal synthase (*phzI*), or the phosphate starvation response regulator (*phoB*)
137 under P-rep (7 mM Pi) or P-lim (100 μM Pi) conditions in 96-well plate liquid cultures (Fig. 2A). The
138 wild type produced phenazines under both conditions but showed markedly higher induction per cell
139 under P-lim. In contrast, the Δ*phzI* mutant failed to produce phenazines under P-lim and P-rep,
140 confirming that QS is required for induction under P-lim. Similarly, the Δ*phoB* mutant did not produce
141 phenazines under P-lim but retained production under P-rep, indicating that phosphate stress signaling via
142 PhoBR is also required in the P-lim response.

143 We next asked whether exogenous addition of the QS signal produced by PhzI would complement Δ*phzI*
144 and whether this response is specific to phosphorus depletion. We performed a dose–response assay by
145 supplementing the Δ*phzI* mutant with the N-(3-hydroxy-hexanoyl)-L-homoserine lactone (3-OH-C6-
146 HSL) (Fig. 2B). *P. synxantha* produces at least six AHLs, including three of the hydroxy form, with 3-
147 OH-C6-HSL having the highest sensitivity to the PhzR.[46] To restrict growth and isolate regulatory
148 effects, we used a defined buffer medium lacking either nitrogen (No-N) or both nitrogen and phosphate
149 (No-N/P). After 20 h, PCA production was absent in No-N cultures, even at high QS signal
150 concentrations, but was strongly induced in No-N/P cultures in a dose-dependent manner.

151 We further asked whether phosphorus limitation increases sensitivity to QS molecules. We therefore
152 performed a second 3-OH-C6-HSL dose–response assay (Fig. 2C), this time allowing the Δ*phzI* mutant to
153 grow under P-rep (7 mM) and P-lim (100 μM) conditions. After 20 h, PCA production was present in
154 both conditions in a dose-dependent manner, but under P-lim, lower QS signal concentrations were
155 sufficient to induce phenazine production. Fitting a two-parameter Hill (log-logistic) function revealed
156 half-maximal effective concentrations (EC50) of 0.51 μM (P-rep) and 0.05 μM (P-lim), indicating ~10-
157 fold greater sensitivity under phosphate stress.

Lastly, to verify QS signal production, we directly quantified AHLs (i.e., 3OH-C6-HSL, 3OH-C8-HSL, and 3OH-C10-HSL) by LC-MS under P-rep, P-lim, and N-lim (nitrogen limited) conditions for both the wild-type strain and Δ*phzI*. Results are shown for WT (Fig. 2D). For the wild-type strain, QS signals were produced under both P-lim and P-rep but were not detected under N-lim. No AHLs were detected with the Δ*phzI* strain. 3OH-C10-HSL was not detected under any conditions. Our limit of detection was 10 nM for all AHLs.

Together, these results demonstrate that phenazine production under P-lim is QS-dependent and requires the PhoBR two-component system. Moreover, phosphate stress sensitizes QS by lowering the AHL activation threshold, enabling induction at levels that are non-inducing under P-rep or N-lim.

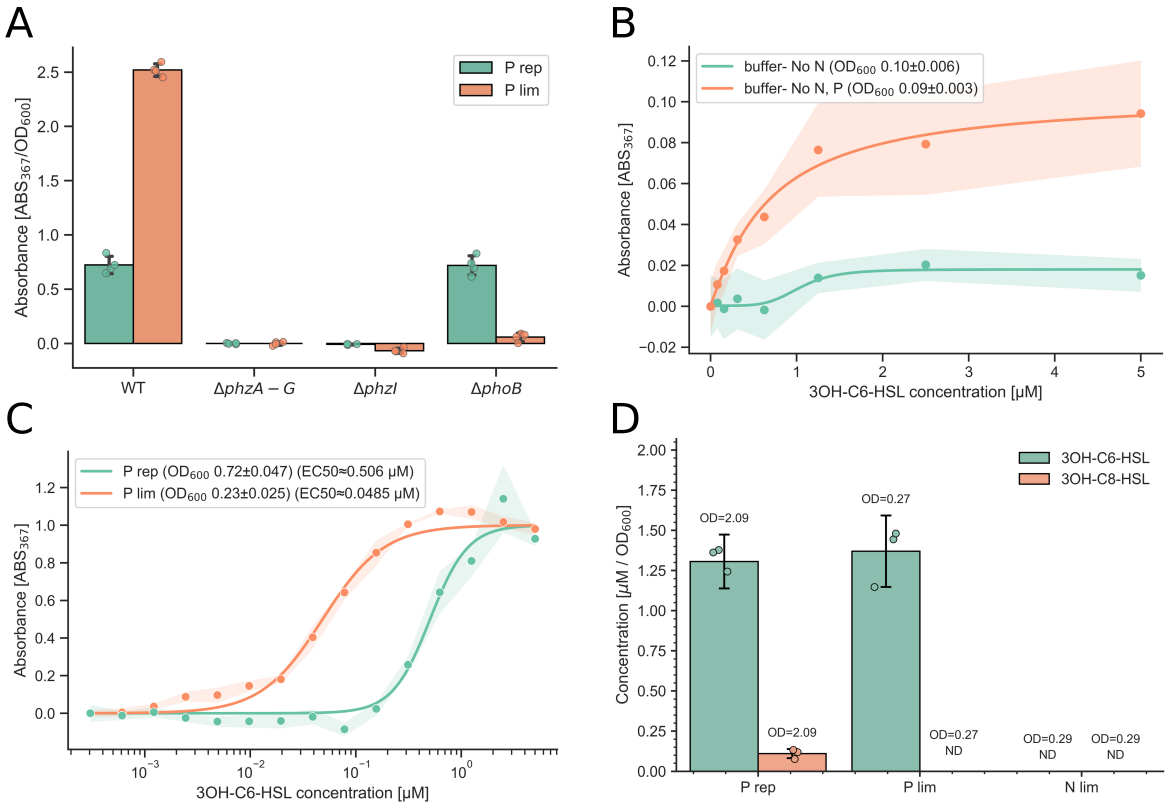

Figure 2: Quorum sensing requirement and reduced AHL concentration threshold for phenazine production in *Pseudomonas synxantha* 2-79 under phosphorus limitation. (A) Phenazine-associated absorbance normalized to cell density ($ABS_{367} \cdot OD_{600}^{-1}$)) in *P. synxantha* strains under phosphorus-replete (P-rep) and phosphorus-limited (P-lim) medium at 20 h post-inoculation. Values were baseline-

172 corrected using the Δ*phzA-G* mutant mean for each condition. Bars show mean ± SD of replicates; points
173 represent individual measurements; n=4. **(B)** Dose–response of the Δ*phzI* mutant strain to exogenous 3-
174 OH-C6-HSL under nitrogen-free (No-N) and combined nitrogen- and phosphorus-free (No-N, P)
175 conditions at 20 h post-inoculation. Responses were baseline-corrected by subtracting the mean signal at
176 0 μM 3-OH-C6-HSL within each condition. Points show per-dose means; shaded regions indicate mean ±
177 SD of replicates; n=5. Curves show four-parameter logistic model fits. Inset in legend: mean ± SD of
178 OD_{600} at the assay timepoint. **(C)** Dose–response of the Δ*phzI* mutant strain to exogenous 3-OH-C6-HSL
179 at 20 h under P-rep and P-lim medium at 20 h post-inoculation. Responses were baseline-corrected and
180 scaled to an empirical E_{max} (median of the two highest doses) to yield 0–1 normalization. Points show per-
181 dose means; shaded bands indicate ±SD across replicates; n=3. Curves are two-parameter Hill fits; Insert
182 in legend: mean ± SD of OD_{600} at the assay timepoint and EC_{50} values from the fits. **(D)** AHL
183 concentration normalized to cell density (μM · OD_{600}^{-1})) for 3OH-C6-HSL and 3OH-C8-HSL across P-
184 rep, P-lim, and nitrogen-limited (N-lim) conditions. Bar plots show mean ± SD. Values above each bar
185 indicate the corresponding optical density (OD_{600}) at sampling time (22 h). "ND" denotes values below
186 the detection limit.

187 **Phosphorus limitation enables quorum sensing activation at low cell densities in planktonic culture**

188 Because QS is required for phenazine production under P-lim, we inferred that phosphate stress decreases
189 the cell-density threshold for QS activation. To test this, we used reporter strains to track QS-dependent
190 induction in wild type *P. synxantha* 2-79 grown in well-mixed liquid culture across phosphate regimes
191 (25, 100, and 7000 μM Pi) with or without exogenous 3-OH-C6-HSL (AHL) (Fig. 3A-B). Our previously
192 constructed P_{phoA} and P_{phzA} reporter strains[48] served to monitor phosphate limitation and phenazine
193 biosynthesis, respectively.

194 P_{phoA} was induced in mid-exponential phase at 25 and 100 μM Pi and was absent at 7000 μM (P-rep), with
195 induction timing and cell density scaling with phosphate availability. Without added AHL (AHL (−)),
196 P_{phzA} was induced in late exponential/early stationary phase under all conditions, but earlier and at
197 substantially lower density in P-lim compared to P-rep (OD_{600} at induction: 25 μM, 0.0846 ± 0.001; 100
198 μM, 0.219 ± 0.005; 7000 μM, 0.806 ± 0.006; mean ± SD), representing ~10-fold and ~4-fold reductions
199 at 25 and 100 μM, respectively. Addition of AHL (AHL (+)) advanced induction time and lowered the
200 density threshold further; under P-lim, P_{phzA} onset aligned more closely with P_{phoA}, consistent with
201 phosphate stress priming the QS response while endogenous signal accumulation is rate-limiting when
202 AHL is not supplied. It is also noteworthy that even when AHL is exogenously added in excess, gene

203 expression still requires the cells to be under P limitation or relatively high cell density under P-rep for
204 induction. That is, it seems that beyond requiring high AHL concentrations the cells need to be a
205 physiologically readiness state (e.g., P stress, other stress responses at high cell density).

206 These results indicate that phosphate stress reduces the cell-density requirement for quorum activation
207 and speeds QS-dependent gene expression in well-mixed cultures, motiving tests in structured
208 environments that better simulate rhizosphere matrices, where mass transfer and bacterial confinement
209 could further tune this sensitization.

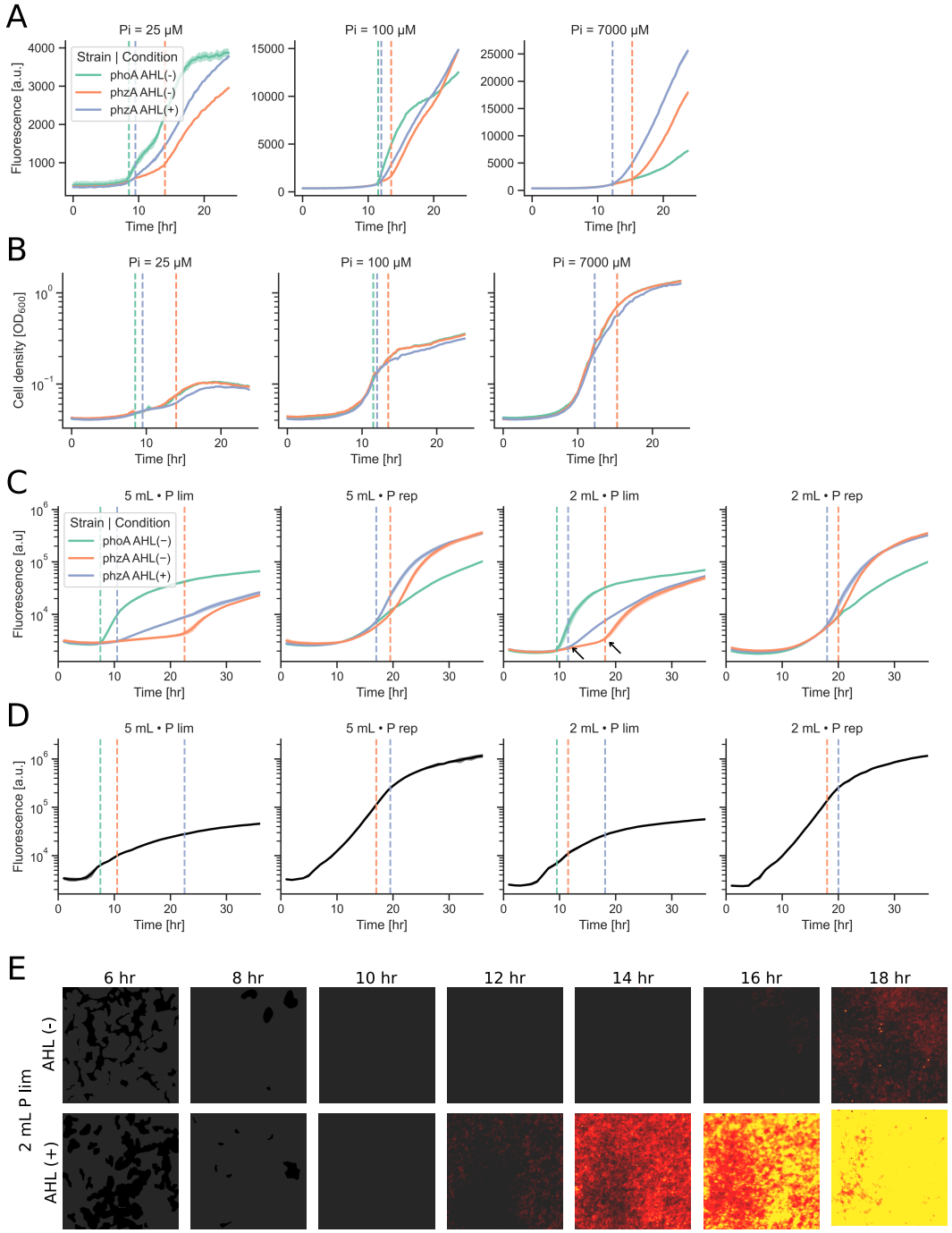

Figure 3: Induction benchmarks and growth dynamics under phosphorus regimes of planktonic and sessile *Pseudomonas synxantha* 2-79 cultures. (A) Induction curves for phosphate-stress (*phoA*) and phenazine biosynthesis (*phzA*) reporters in liquid cultures across phosphate regimes (Pi = 25, 100, 7000 μM). Raw fluorescence intensity values are shown. **(B)** Growth curves in liquid cultures as cell density (OD_{600}). **(C)** Induction curves for *phoA* and *phzA* in agar biofilms under P-lim and P-rep conditions in either 5 mL or 2 mL agar volumes. Raw fluorescence intensity values are shown. **(D)** Growth curves in agar biofilms represented by the constitutive reporter fluorescence intensity (cell

density proxy). **(E)** Representative images of reporter induction time course for biofilms grown under P-lim in a 2 mL agar volume. Intensity of fluorescence is depicted by red to yellow hue. Gray shading denotes the area coverage of aggregates. Legend: WT P_{phoA} without AHL addition (green), WT P_{phzA} without AHL addition (orange), P_{phzA} with AHL addition (blue). Curves denote mean; shading denotes ± SD; n = 3. Error not seen is smaller than the line. Dashed vertical lines mark reporter induction times. Arrow on third graph correspond to images in (E)

Phosphorus limitation also lowers the cell density threshold for QS activation in sessile populations

We employed an early-stage colony–biofilm assay using our previously developed imaging system[48] to quantify growth and reporter expression in *P. synxantha*. In this diffusion-dominated context, AHL local concentrations arise from the balance between signal production, diffusive loss into the underlying agar (which serves as a sink), and retention within the biofilm matrix. Reporters P_{phoA} (phosphate stress) and P_{phzA} (phenazine production) tracked induction, and a constitutive reporter provided a proxy for cell density (Fig. 3C-E). By varying nutrient status, agar volume, and AHL supplementation, we modulated regulatory sensitivity, sink strength (5 mL vs 2 mL agar volumes), and signal availability, respectively, to reveal how these factors shape QS activation.

5 mL agar: Under P-lim, *phoA* was detected early (~7.5 hr), but *phzA* induction was markedly delayed (~22.5 hr). Under P-rep, *phoA* did not induce (as expected), whereas *phzA* induced at 19.5 h. This pattern is opposite to planktonic cultures, where P-lim induces earlier than P-rep, indicating that in the structured, diffusion-dominated context, QS-signal accumulation is delayed under P-lim. Notwithstanding the delay, the biofilm density required for QS-mediated *phzA* activation was ~9-fold lower under P-lim than P-rep (constitutive reporter [a.u.]: P-lim 27,852 ± 1,207; P-rep 248,856 ± 13,115; mean ± SD), which is consistent with planktonic trends.

2 mL agar: Under P-lim, *phoA* was detected early (~9.5 hr), *phzA* induction occurred (~18 hr; earlier than 5 mL condition), and before P-rep (~20 hr), suggesting that QS-signal thresholds were achieved more rapidly when sink strength was reduced (shallower agar). Interestingly, the biofilm density at the moment

244 of *phzA* induction was nearly identical between the 2 mL and 5 mL conditions for both P-lim and P-rep,
245 even though the timing differed. As in 5 mL agar (and consistent with planktonic data), P-lim required
246 ~10-fold lower density than P-rep for QS-mediated *phzA* activation.

247 Exogenous AHL caused P-lim colonies to induce *phzA* expression rapidly—coincident with the onset of
248 phosphate stress—bypassing the need for signal accumulation through growth. AHL rescue in P-rep
249 colonies also accelerated induction but still required higher density than P-lim. These results are again
250 consistent with liquid cultures: the fact that induction still required a physiological state primed for
251 induction (i.e., P limitation, high biofilm density) rather than inducing independently of P stress or high
252 density when excess exogenous AHL is provided, supports the idea that phosphate stress provides
253 competence for the QS system.

254 These results highlight an interplay of nutrient status and biofilm QS signal accumulation as influenced
255 by the diffusive environment. Phosphorus limitation lowers the biofilm density required for QS
256 activation, but induction still depends on local signal concentration, which is influenced by retention
257 within the colony versus loss into the agar.

258 **Phosphorus stress and spatial confinement accelerate QS in soil-like microenvironments**

259 To examine how environmental structure shapes local signal concentration and QS activation, we
260 employed a previously designed microfluidic platform[64] that mimics soil-like conditions where
261 confinement and mass transfer limitation can be modulated to affect signal concentration (Fig. 4A). Low-
262 density cultures (OD_{600} = 0.05) of a dual reporter strain (*P. synxantha* 2-79 P_{tac}-P_{phzA}) were inoculated, and
263 air was introduced to create a heterogeneous landscape of water pockets that varied in size and
264 connectivity (Fig. 4B–C). Biomass and *phz* induction were tracked via the constitutive (P_{tac}-mCherry, red
265 channel) and inducible (P_{phzA}-GFP, green channel) reporters, respectively, across roughly 50 regions of
266 interests (ROIs) imaged in the reactor (Fig. 4E).

267 Across these microenvironments, induction timing under P limitation was strongly dependent on local
268 cell density scaling with a power-law relationship and generally coincided with water saturation (Fig.
269 4D). Regions with lower saturation tended to have higher local cell densities, and in such confined
270 pockets induction occurred rapidly (Fig. 4F; 3.4 h ± 1.0 h, mean ± SD). In contrast, high-saturation and
271 lower density regions showed delayed induction, likely due to a higher initial phosphate availability per
272 cell prior to depletion. Interestingly, while high-density regions induced earlier, their induction curves
273 were more gradual in comparison to low density regions, suggesting heterogeneous activation among
274 smaller, disconnected water pockets within the same ROI. Highly saturated regions, by contrast, induced
275 later but with steeper, more synchronized activation curves, consistent with larger, connected liquid
276 domains within the ROI (Fig. S2).

277 In P-replete experiments, induction is markedly delayed (23.6 h ± 4.3 h; mean ± SD), reinforcing the
278 observation that phosphate stress lowers the effective activation threshold and promotes earlier induction
279 in confined microenvironments (Fig. 4F). This scaling therefore highlights how nutrient stress and spatial
280 confinement together modulate effective signal concentration, enabling QS activation. It is worth noting
281 that under P-rep, oxygen likely became a limiting nutrient (suspected due to lack of growth near center of
282 water pockets), and therefore because of this complexity the induction times were broad between ROIs
283 and excessively delayed under P-rep.

284 Taken together, these data demonstrate that the combination of phosphorus stress and spatial confinement
285 enables QS activation in microenvironments that would otherwise restrict signal buildup. We next asked
286 whether lowered QS concentration thresholds could provide an ecological advantage in a community
287 setting.

288

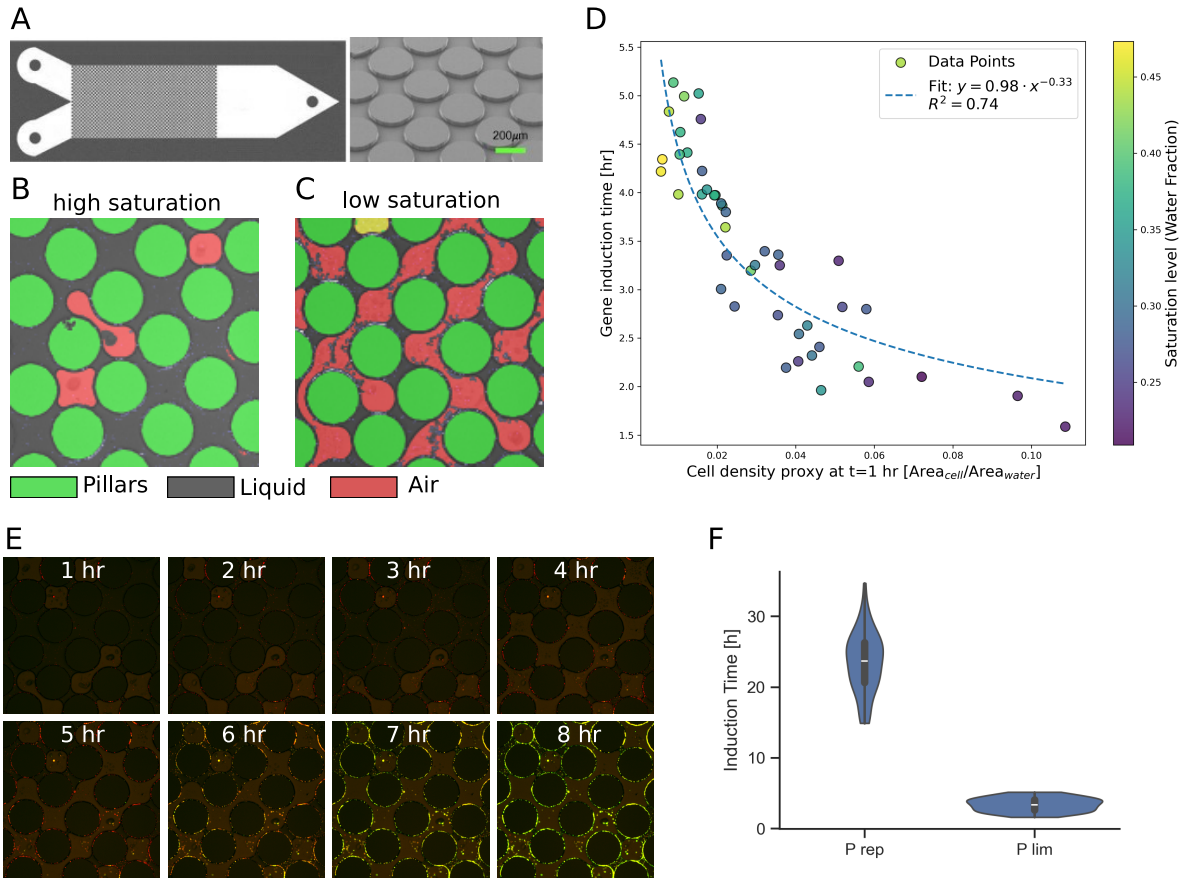

Figure 4: Relationship between cell density, water saturation, and *phz* induction time in microfluidic microenvironments. (A) Schematic (left) and scanning electron micrograph (right) of the synthetic porous platform used to create spatially structured microenvironments. The device contains cylindrical pillars (200 µm diameter) arranged in a hexagonal lattice, generating defined pore spaces. The depth of the device is 10 µm. **(B, C)** Representative images of pore-scale water distribution at high saturation (B) and low saturation (C), with pillars shown in green, water-filled pores in gray, and air-filled pores in red. **(D)** Relationship between cell density in pore water (x-axis; area fraction of cells in water-filled regions at t = 1 h) and gene induction time for the P_{phzA} reporter (y-axis) under P-lim. Points are colored by water saturation level as indicated by the heat map (fraction of pore volume filled with water). Dashed line shows a power-law fit. Data represent pooled technical replicates from regions in the reactor; n = 45. **(E)** Representative overlayed images of reporter induction (constitutive: red, *phzA*: green) over time. **(F)** Distribution of induction times (h) under P-lim (same data from (D)) and P-rep. Violins show kernel density; the embedded box marks the interquartile range with a line at the median. Technical replicates: P-lim n=45, P-rep n=50.

Phosphorus limitation confers cooperative and antagonistic QS driven community dynamics

Under nutrient stress, microbial communities can flip between cooperative information exchange (e.g., quorum signals) and antagonistic interference (e.g., antibiotics), reshaping which partners win or lose.

307 To determine whether phosphorus limitation broadly enhances AHL production and promotes cross-talk
308 among *Pseudomonas* species, we assembled a panel of rhizosphere-associated strains representing both
309 close relatives of *P. synxantha* and more distantly related pseudomonads. Each strain was grown under N-
310 lim, P-lim, or P-rep conditions, cell-free supernatants were then collected to challenge the *P. synxantha*
311 Δ*phzI*–P_{phzA} reporter, which cannot synthesize AHLs but fluoresces upon QS activated *phzA* expression
312 (Fig. 5A). Supernatants from multiple donors activated the reporter, with the strongest and broadest
313 induction under P-lim and P-rep, and little to none under N-lim. As expected, controls with the Δ*phzI*
314 donor did not induce, whereas the wild-type donor triggered a robust response. Notably, across the panel,
315 strains carrying homologous *phzIR* operons consistently induced *phzA* under P-lim, suggesting that
316 phosphate stress broadly elevates AHL output among *Pseudomonas* species. In contrast, *P. aeruginosa*
317 PA14 failed to induce the reporter, consistent with its production of 3-oxo-acyl-HSLs rather than the 3-
318 hydroxy-acyl-HSL(s) recognized by PhzR in *P. synxantha*.

319 Next, we asked whether QS activation under P-lim alters microbial interactions within competitive
320 communities under oxic conditions where phenazines primarily function as antibiotics.[11] We performed
321 co-culture assays between *P. synxantha* (wild type and Δ*phzA-G*, a phenazine-null mutant) and
322 *Pedobacter kyonggii*, a common rhizosphere isolate. When P-limited, the wild-type strain significantly
323 suppressed *P. kyonggii* growth, whereas the Δ*phzA-G* mutant did not (Fig. 5B). This phenazine-linked
324 advantage was absent under N-lim in the wild-type strain and, interestingly, under P-rep conditions as
325 well. Although the wild type produced PCA under P-replete conditions, induction occurred much later
326 (~35 h vs ~16 h in P-lim; see Fig. S5), by which time the co-cultures had already completed most of their
327 growth, leaving little opportunity for inhibition to manifest. Thus, the phenotype likely reflects the timing
328 of phenazine onset relative to culture growth.

329 These findings indicate that phosphorus limitation broadly elevates AHL signaling across *Pseudomonas*
330 spp., priming QS in *P. synxantha*. Moreover, phenazine production under phosphorus stress suppresses
331 growth of *P. kyonggii*.

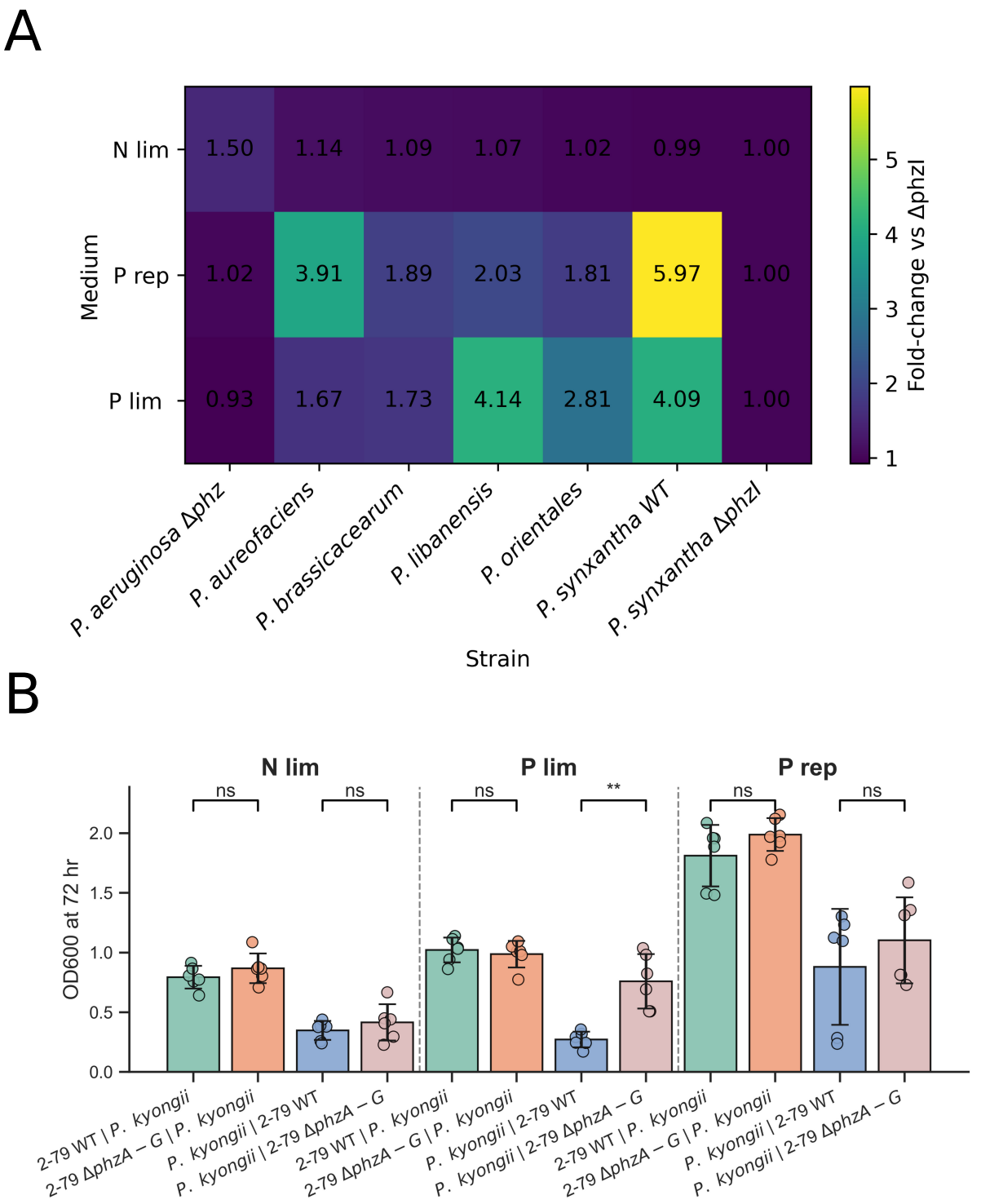

Figure 5: (A) *Pseudomonas* spp. supernatant cross-induction QS assay. Heatmap of fluorescence induction in *P. synxantha* Δ*phzI*-P_{phzA} across supernatants of selected strains and media conditions at 24 h. Rows represent media (N-lim, P-lim, P-rep); columns are strain supernatants. Each cell shows the fold-

336 change of the chosen metric relative to the reference strain, *P. synxantha* Δ*phzI*, within the same medium.
337 Where shown, numeric labels are fold-change values rounded to two decimals; the *P. synxantha* Δ*phzI*
338 column equals 1 by definition. Fluorescence is normalized by OD600. (mean, $n = 6$) **(B) Competition**
339 **assays between *P. synxantha* against *Pedobacter kyonggii* under various nutrient regimes**. Bar plots
340 show OD600 at 72 h (mean ± SD, $n = 6$) for four pairings. The first name indicates the strain measured;
341 the second is its pairing partner. Results are shown separately for N-lim, P-lim, P-rep media. *P. synxantha*
342 wild type (2-79 WT) and *P. synxantha* Δ*phzA-G* (2-79 Δ*phzA-G*). Statistical comparisons use Welch's *t*-
343 test; brackets denote significance (ns, not significant; ** $p < 0.01$).

344

345 **Discussion**

346 Our study reveals that phosphorus limitation rewires the quorum-sensing (QS) circuitry of *Pseudomonas*
347 *synxantha* 2-79, lowering the effective signal concentration required for autoinduction and enabling
348 phenazine biosynthesis at conditions corresponding to much lower densities (OD ≈ 0.08 in liquid
349 cultures). Phosphate stress reduces the acyl-homoserine lactone (AHL) concentration required for
350 activation by roughly an order of magnitude under our tested conditions, thereby heightening cellular
351 sensitivity to QS signals. This response depends on the PhoBR two-component system: inactivation of
352 PhoBR abolishes phenazine induction even when AHL levels are high, demonstrating that phosphate
353 stress provides a necessary regulatory input. In structured habitats, where mass transfer alters QS
354 molecule accumulation, phosphate limitation emerges as a key modulator of QS activation. In colony
355 biofilms, phenazine induction times under P limitation are strongly affected by agar volumes and biofilm
356 density, implicating biofilm retention and diffusive losses in achieving threshold AHL concentrations.
357 Exogenous AHL addition collapses this concentration requirement but still requires a physiological state
358 primed for induction (i.e., P limitation or higher cell densities under P replete). Confinement in
359 micropores creates microenvironments that retain signals and enable localized QS activation, again
360 showing that physical structure and nutrient state jointly set QS thresholds. These environmentally-tuned
361 threshold shifts have ecological consequences. Under phosphate limitation, *P. synxantha* inhibits growth
362 of the rhizosphere isolate *Pedobacter kyonggii* through phenazine production, a benefit lost in the
363 phenazine-null mutant and under nitrogen limitation or phosphate-replete conditions. Early phenazine

364 synthesis may thus serve dual functions in resource competition and phosphate acquisition, coordinated
365 through stress-responsive signaling.

366 Our data argue against "concentration-only" or "density-only" views and instead support an AND-gate
367 model for QS activation: (i) sufficient signal accumulation (production versus diffusion, advection,
368 sorption, and decay) to cross a threshold and (ii) a physiological readiness state that licenses
369 responsiveness. Density remains a useful proxy because per-cell production scales with biomass and high
370 density often coincides with competence, but other regulatory programs can shift the effective threshold,
371 explaining low-density induction under nutrient stress. In our system, QS signal responsiveness is tunable
372 by nutrient status, PhoBR under phosphate limitation, so signal is necessary but not sufficient. This
373 framework reconciles our observations: under P-replete + excess AHL, low-density cultures fail to induce
374 despite ample signal, indicating physiological unreadiness; responsiveness emerges by mid- to late-
375 exponential growth as global regulators (e.g., Gac/Rsm) and stress programs rise. Under P limitation,
376 induction synchronizes with phosphate stress. Exogenous AHL enables induction at comparatively lower
377 cell densities, with the activation density tunable by the imposed Pi level. Again, though, induction did
378 not occur until P limitation was achieved.

379 This model aligns with prior work. Overactivation of the stringent response via RelA in *P. aeruginosa*
380 prematurely activates RpoS, LasR, RhlR and autoinducer synthesis, driving LasB production independent
381 of density, i.e., physiological readiness upstream of signal thresholds.[65] Exogenous PQS (an autoinducer)
382 addition can override cell-density dependence but not growth-phase dependence, underscoring the
383 physiological readiness requirement.[66] More broadly, nutrient limitation and growth rate jointly modulate
384 extracellular signal accumulation across species, with phosphate and sulfur limitation disproportionately
385 elevating alkylquinolones even at lower OD.[67] Our findings extend this signal-accumulation +
386 physiological readiness concept by showing that native PhoBR directly sensitizes an unmodified AHL-
387 based QS network in a rhizosphere pseudomonad, reframing QS as an environmentally tuned
388 concentration-sensing mechanism whose effective activation threshold is set jointly by autoinducer

389 concentration and regulatory state. Related frameworks[43] reach similar conclusions; nevertheless,
390 proliferating new labels for QS risks semantic confusion that can imply a single dominant driver.[36]
391 Instead, we favor a generalizable AND-gate view that explains QS outputs in sparse, fragmented soils and
392 highlights practical levers (e.g., nutrient availability, confinement, and mass transfer) for engineering
393 compatible microbial communities and biosensors in heterogeneous environments.

394 **Methods:**

395 **Bacteria.** The primary strain was *Pseudomonas synxantha* (formerly *P. fluorescens*) 2-79 WT. Isogenic
396 derivatives included Δ*phzI* (AHL synthase null), Δ*phzA-G* (phenazine-null), and Δ*phoB* (phosphate-stress
397 response regulator null). Reporters carrying transcriptional fusions included P_{phzA}–mNeonGreen
398 (QS/phenazine biosynthesis), P_{phoA}–mNeonGreen (phosphate stress), P_{phzA}–GFP, P_{tac}–mCherry
399 (QS/phenazine biosynthesis, constitutive density proxy) and $P_{PA10403}$-mNeonGreen (constitutive density
400 proxy). Donor/competitor strains for crosstalk and competition assays included *Pseudomonas*
401 *aureofaciens* 30-84, *P. brassicacearum* 106, *P. libanensis* 84, *P. orientalis*, *P. aeruginosa* Δ*phz1/2* and
402 *Pedobacter kyonggii*. Sources, identifiers, and genotypes are listed in Table S2.

403 **Culture conditions.** Unless noted, overnight cultures of *Pseudomonas* strains were propagated at 30 °C,
404 250 rpm in LB (Miller) for 16-18 h; *E. coli* DH10B/SM10 were grown at 37 °C. Experimental assays
405 used defined MOPS medium (below). Antibiotics were used only for selection (gentamicin 30 μg mL^{-1},
406 tetracycline 15 μg mL^{-1}). All experiments with reporters were antibiotic-free. Strains were stored as −80
407 °C glycerol stocks (20% v/v) and streaked fresh for each experiment.

408 **Media compositions and nutrient-regime definitions**

409 **MOPS defined medium.** Per liter: 25 mM MOPS (pH 7.0; adjusted with 1 M NaOH), 55.5 mM glucose,
410 16 mM NH_4Cl, 7 mM KH_2PO_4, 0.41 mM $MgSO_4 \cdot 7H_2O$, 0.68 mM $CaCl_2 \cdot 2H_2O$, Aquil-based trace
411 metals[68] with Fe 10 μM and EDTA 100 μM. KH_2PO_4 7 mM (P-rep/N-lim) or 25–100 μM (P-lim); NH_4Cl

412 16 mM (P-rep/P-lim) or 2 mM (N-lim). No-N and No-N/P buffers omitted NH_4Cl and NH_4Cl/KH_2PO_4,
413 respectively. MOPS agar consisted of MOPS medium with 1.0% (w/v) noble agar.
414 **Plant medium.** 0.5× MS (Sigma-Aldrich M5519), 0.6% (w/v) Phytagel (Sigma-Aldrich P8169), pH 5.8
415 (KOH); P-lim omits KH_2PO_4.
416 **Phosphate-sorbing (P-HFO) condition.** Hydrous ferric oxide (HFO) was synthesized, phosphate was
417 then sorbed and sequestered (P-HFO). P-HFO was added to phosphate deficient plant medium (see
418 below) at 1.6 g/L. See Note S1 for P-HFO preparation.
419 **MES defined medium.** Per L: 50 mM MES pH 5.8 (KOH), 50 mM sucrose, salts as above. KH_2PO_4 7
420 mM (P-rep/N-lim) or 100 µM (P-lim); NH_4Cl 16 mM (P-rep/P-lim) or 2 mM (N-lim).

421 **Reporter and mutant generation and verification**

422 Transcriptional fusions were constructed using the mini-Tn7 system.[69] Promoter (P_{phzA}) was cloned
423 upstream of mNeonGreen in pJM220 by Gibson assembly and transformed into *E. coli* DH10B.
424 Gentamicin-resistant transformants (30 µg mL^{-1}) were verified by colony PCR and Sanger sequencing.
425 Mini-Tn7 elements and pTNS1 helper (TnsABCD; delivered from *E. coli* SM10/pTNS1) were introduced
426 into electrocompetent *P. synxantha* 2-79. Transconjugants were selected on LB-gentamicin and screened
427 by junction PCR for single-copy insertion at attTn7 (downstream of *glmS*). Reporter function was
428 validated in plate-reader assays (P_{phzA} induction under QS-permissive conditions). Plasmids and primers
429 are listed in Tables S3–S4.

430 In-frame deletion mutants were constructed using a suicide plasmid. Approximately 1-kb regions
431 upstream and downstream of *phzA-G* and *phzI* were PCR-amplified and assembled with SmaI-digested
432 pEX18Gm by Gibson assembly. The plasmid was electroporated into *E. coli* DH10B, and transformants
433 were selected on LB agar with gentamicin (30 µg mL^{-1}). Correct constructs were verified by PCR and
434 introduced into *P. synxantha 2-79* wild-type strains via triparental conjugation. Merodiploids were
435 selected on Vogel–Bonner minimal medium (VBMM) containing gentamicin (30 µg mL^{-1}), followed by

436 counter-selection on sucrose medium (5 g L^{-1}yeast extract, 10 g L^{-1}tryptone, 100 g L^{-1}sucrose). Colonies
437 in which homologous recombination was successful were identified by PCR. Deletions were confirmed
438 by diagnostic PCR across the targeted loci and by phenotype: Δ*phzA-G* lacked ABS367nm (PCA proxy)
439 signal and lacked phenazine product, verified via LC-MS analysis. Δ*phzI* required exogenous AHL for
440 induction and lacked AHL production via LC-MS/MS analysis.

441 **Plant-microbe reporter induction assay**

442 *Brachypodium distachyon* Bd21-3 seeds were dehusked, sterilized with chlorine gas (see Note S2), plated
443 on 0.6% Phytagel with 0.5× MS, and vernalized (4 °C, 4 d). Seedlings were grown 2 d (16 h light/8 h
444 dark, 25 °C), then immersed 30 min in 0.5× MS lacking phosphate (P-lim) containing *P. synxantha* 2-79
445 at OD_{600} = 0.1. Seedlings were transferred into 1 cc syringes filled with 0.6% Phytagel prepared with 0.5×
446 MS under the indicated phosphate condition (P-lim, P-rep, or P-HFO) and incubated vertically for 2 d
447 prior to imaging.

448 Seedlings embedded in phytagel mounted so that roots+phytagel were submerged in sterile 0.5× MS
449 buffer. Imaging used a Zeiss Lightsheet Z.1 with EC Plan-Neofluar 5×/0.16 air objective. Dual-channel
450 acquisition captured GFP/mNeonGreen (488 nm ex, 498 nm em) and mCherry (561 nm ex, 571 nm em)
451 on separate cameras with a dual-band emission filter (Zeiss LBF 488/561). Z-stacks were collected at 5
452 µm step, XY pixel 0.93 µm, 100 ms exposure per slice; laser power was held constant across conditions
453 (20% at 488 and 561 nm). Maximum intensity projections (MIPs) were generated for analysis.

454 All analysis used Fiji/ImageJ with a custom macro. Red channel (P_{tac}–mCherry) was median-filtered (r =
455 4), background-subtracted (rolling ball 50 px), converted to 8-bit, and locally thresholded (Bernsen, r =
456 15) to build masks. Objects were defined by particle analysis (min size 20 px) and applied to original
457 red/green images to extract integrated density (IntDen) and area. Mean intensity per object was computed
458 as IntDen/area for both channels. CSVs were exported for Python analysis.

459 **Planktonic 96-well kinetic experiments**

460 Overnight cultures of *P. synxantha* 2-79 (WT, Δ*phzA-G*, Δ*phzI*, Δ*phoB,* Δ*phzI*–P_{phzA}) were washed 3× in
461 MOPS containing 10 µM phosphate, and inoculated into 96-well plates at OD_{600} = 0.01. Plates were
462 incubated in a Tecan Spark 10M (30°C; orbital shaking amplitude 2.5 mm, 216 rpm) with reads every 15
463 min for 24 h. OD_{600} was read at 600 nm; ABS367 was read at 367nm for PCA-associated absorbance;
464 mNeonGreen at Ex/Em 485/535 nm. Induction time was approximated from fluorescence time series by
465 manual curation. ODs at induction were obtained by linear interpolation of OD_{600} (t) at that time.

466 For the AHL-supplemented dose-response assays, 3-OH-C6-HSL (Adipogen; ≥98%) stock was prepared
467 with methanol (final solvent ≤0.02% v/v; vehicle controls showed no effect from solvent carryover). Dose
468 ranges spanned sub-nM to tens of µM (specified per figure).

469 For the no-growth supplementation assay, Δ*phzI* overnight culture was washed (3×) in the respective
470 treatment buffer (No-N or No-N/P) were inoculated at OD_{600} = 0.1. For the growth-permissive
471 supplementation assays, Δ*phzI* overnight culture was washed (3×) in MOPS containing 10 µM phosphate
472 and inoculated at OD_{600} = 0.01. Responses were baseline-corrected to 0 µM within condition and fit with
473 a two-parameter Hill (log-logistic) model (top = 1, bottom = 0) to estimate EC_{50} with 95% CIs.

474 **AHL quantification by LC–MS/MS**

475 Overnight cultures of *P. synxantha* 2-79 (WT, Δ*phzI*) were washed 3× in MOPS, then grown in glass
476 culture tubes (30 °C, 250 rpm) under P-rep, P-lim, and N-lim conditions for 22 h. Cultures were then
477 pelleted, supernatants were collected, filtered through a 0.22 µm PES filter, diluted 1:1 in methanol,
478 incubated for 1 h at -20°C, pelleted, then supernatants were collected before analyzing.

479 Analytical standards (3-OH-C6-HSL, 3-OH-C8-HSL, 3-OH-C10-HSL, and 3-oxo-C8-HSL; ≥95–98%
480 purity; Adipogen/Cayman) were prepared by solubilizing powders in methanol as 1-10 g L^{-1} primary

481 frozen stocks (-20 °C). A 100 µM all analyte mix was made in methanol with 0.1% formic acid.
482 Calibration standards were prepared by diluting the analyte mix in methanol with 0.1% formic acid.

483 A Waters (Milford, MA) Acquity Premier UPLC was fitted with a HSS T3 column and coupled to a Xevo
484 Q-TOF G2S. Mobile phase A was 0.1% formic acid in water and mobile phase B was 100% acetonitrile.
485 The initial mobile phase composition was 2.5 % B for 0.5 minutes with a linear gradient to 95% B ending
486 at 5 minutes. After a 0.5 minute hold (5.5 min) the composition was returned rapidly to the initial
487 conditions (5.6 min) and held for an additional 0.25 minutes (to 5.74 minutes). The gradient was cycled
488 without interruption during any acquisition. The flow rate was held constant throughout at 0.3 mL/min,
489 the samples held at 10 °C, the column temperature maintained at 40 °C, and the injection volume was 4
490 µL. The 2.1 mm × 50 mm × 1.8 µm column was used without a guard column.

491 The ion source block was held at 120 °C, capillary voltage was 3 kV, desolvation gas flow and
492 temperature were 600 lph and 500 °C, the cone gas flow as 15 lph, and the source offset was 80 V.
493 Separate mass spectral data sets were collected in both MS mode from 50-1200 m/z and using scheduled
494 MS2 for parallel reaction monitoring of the individual targeted analytes. MS data was acquired in positive
495 sensitivity mode (approximately 18,000 resolution). The mass axis was calibrated against sodium formate
496 and was confirmed daily. Leucine enkephalin was used as lock mass reference during acquisition.

497 Targeted analysis was performed using the Quanlynx program within the Masslynx software suite used to
498 operate the instrument.

499 **Sessile early-stage colony biofilm experiments**

500 Overnight cultures of *P. synxantha* 2-79 (WT, P_{phoA}, P_{phzA}, $P_{PA10403}$) were washed 3× in MOPS containing
501 7 mM phosphate and adjusted to OD_{600}= 0.05. A 5 µL droplet was spotted onto agar plates, air-dried 1 h,
502 and placed in a custom humidity-controlled platform. The agar plates contained either 2 mL or 5 mL of
503 agar. For P-lim plates, phosphate was omitted from the MOPS agar; the only source of phosphate was the

504 5 μL inoculation drop that contained 7 mM phosphate. P-rep consisted of MOPS agar at 7 mM. Images
505 were acquired hourly for 36 h.

506 Time-lapse imaging of bacteria was performed using a previously reported complex-field and
507 fluorescence microscopy system based on the aperture scanning technique (CFAST).[48] Samples were
508 mounted in a 12-well plate and positioned on a motorized XY scanning stage (Thorlabs MLS203-1) to
509 enable automated, parallel scanning of multiple wells.

510 To minimize evaporation of the growth medium during the two-day imaging experiments, the 12-well
511 plate was placed in a custom 3D-printed holder containing wet paper towels to maintain high local
512 humidity. To maintain focus while minimizing photobleaching and phototoxicity, 0.5-μm red fluorescent
513 beads (580/605 nm, ThermoFisher F8812) were pre-mixed with the bacterial suspension at a $1:10^5$
514 dilution from stock. These beads served as markers for focal plane tracking. The beads were excited with
515 a 568 nm laser (Coherent Sapphire 568 LP), and the emitted fluorescence was filtered using a dichroic
516 mirror (Semrock Di01-R488/561) and a bandpass filter (Semrock FF01-R523/610).

517 A 488 nm laser (Thorlabs LP488-SF20G) was used both for complex-field illumination and for excitation
518 of mNeonGreen fluorescence. The complex field data comprising both amplitude and quantitative
519 phase was used to quantify the area coverage of bacterial colonies. Fluorescence intensity was extracted
520 from the mNeonGreen images and subsequently normalized using brightfield images to compensate for
521 variations in excitation power due to differences in medium thickness across the sample.

522 **Microfluidic soil-analog reactor experiments**

523 Devices followed a silicon-etched porous design[64] and fabrication process (see Note S3). Overnight
524 culture of *P. synxantha* 2-79 (dual reporter, P_{phzA}-P_{tac}) was washed 3× in MOPS P-lim (100 μM) or P-rep
525 medium and adjusted to OD_{600}= 0.05 for inoculation into the reactor. Cells were inoculated at a flow rate
526 of 0.1 mL min^{-1} for 3 minutes. Air was then injected and generated heterogeneous water saturation

527 (connected high-saturation domains vs confined pockets). After initial displacement, air was continuously
528 injected at a flow rate of 0.01 mL min^{-1}. Imaging was conducted for 16-40 h depending on experiment.

529 All imaging was performed on a Nikon Ti2 widefield epifluorescence microscope. Time-lapse series used
530 a Plan Apo 20×/0.75 dry objective. GFP was excited with a 488-nm LED and collected with a FITC filter
531 set; mCherry was excited with a 561-nm LED and collected with a TRITC filter set. Images were
532 collected every hour from multiple stage positions.

533 Custom MATLAB code was used to segment bacterial cells based on the red channel (constitutive
534 reporter) and pockets of air based on the green channel (induction of phenazine production). To identify
535 cells, background subtraction was applied to the original image followed by thresholding using a fixed
536 intensity value. Objects smaller than 5px were discarded. To segment pockets of air, we first identified
537 and removed signal from induction, which would otherwise interfere with the detection. For this we
538 segmented fluorescing cells by simple thresholding, expanded their area by dilation (10px) and then
539 replaced intensity values within this area with the background intensity. Following this, air pockets were
540 segmented by smoothing and background subtraction followed by thresholding. Areas smaller than
541 1000px were discarded and holes within air pockets smaller than 50000px were closed. When necessary,
542 segmentation of air pockets was corrected manually. Intensity ratios were based on background-corrected
543 intensities. Induction time vs cell density was fit to a power-law model using log–log linear regression;
544 goodness-of-fit (R^2) and CI on parameters are reported.

545 **Supernatant cross-induction assay**

546 Overnight cultures of *Pseudomonas* strains were washed 3× in MOPS (P-lim and N-lim) medium and
547 inoculated at OD_{600} =0.01 into glass culture tubes (30 °C, 250 rpm) under P-rep, P-lim, and N-lim
548 conditions for 22 h. Cultures were then pelleted, and supernatants were collected and filtered through a

549 0.22 µm PES filter. The cell-free supernatant was then mixed 1:1 with appropriate medium (i.e., P-rep, P-
550 lim, N-lim) for cross-induction assay.

551 An overnight culture of *P. synxantha* 2-79 Δ*phzI*-P_{phzA} was washed 3× in MOPS (P-lim and N-lim) and
552 inoculated at OD_{600} =0.01. A 96-well plate assay was then conducted with the cell-free supernatant
553 mixture following the "Planktonic 96-well kinetic experiments" parameters. Fold-change for RFU/OD_{600}
554 relative to the reference strain *P. synxantha* Δ*phzI* within each medium was then computed. The resulting
555 scores were plotted as a single heatmap.

556 **Pairwise competition assays**

557 Co-culture growth and induction dynamics were monitored using a two-chamber co-culture system that
558 allows fluidic exchange while physically separating populations (Duet Co-Culture System, Cerillo). *P.*
559 *synxantha* (WT or Δ*phzA-G*) and *P. kyonggii* overnight cultures were washed 3× in MES (P-lim and N-
560 lim) medium. Cells were then loaded to either side of the chamber at a starting OD_{600} of 0.01 under N-lim,
561 P-lim, or P-rep media. Duets have the footprint of a 96-well plate, thus the assay was conducted following
562 "Planktonic 96-well kinetic experiments" instrument parameters. Phenazine-dependent suppression was
563 assessed by comparing WT vs Δ*phzA-G*. Statistics used Welch's t-test with two-sided $\alpha = 0.05$. Note that
564 competition assays were run in MES-defined medium (pH 5.8) with sucrose as the carbon source. Sucrose
565 was chosen because *P. synxantha* 2-79 does not utilize it; on glucose, *P. synxantha* rapidly overgrows
566 *Pedobacter kyonggii*, obscuring interaction effects. Using sucrose maintains competitive viability of *P.*
567 *kyonggii* and shifts *P. synxantha* toward relying on metabolites released by P. *kyonggii*, enabling
568 resolution of phenazine-dependent outcomes. The pH was set to 5.8 (buffered with MES) to approximate
569 mildly acidic rhizosphere conditions and because PCA is more membrane-permeant—and thus more
570 potent—at lower pH.

Acknowledgements:

We acknowledge the Resnick Ecology and Biosphere Engineering Facility and Caltech Biological Imaging Center for the training and use of confocal and light sheet fluorescence microscopes. We are grateful to the Resnick Sustainability Institute for enabling resources and financial support. R.E.A. was supported by an NSF Postdoctoral Research Fellowship in Biology (Grant No. 2209379).

Author contributions: R.E.A., and D.K.N. designed research; R.E.A., H.J., O.Z., R.L.A., and N.D. performed research; R.E.A., H.J., O.Z., R.L.A., and N.D. analyzed data; and R.E.A., H.J., O.Z., R.L.A., N.D., D.M., C.Y., and D.K.N. wrote the paper.

References:

1. Mavrodi, D.V., Blankenfeldt, W., Mavrodi, O.V., Weller, D.M., and Thomashow, L.S. (2025). Microbial phenazines: biosynthesis, structural diversity, evolution, regulation, and biological significance. Microbiology and Molecular Biology Reviews *0*, e00147-23. https://doi.org/10.1128/mmbr.00147-23.

2. Dahlstrom, K.M., McRose, D.L., and Newman, D.K. (2020). Keystone metabolites of crop rhizosphere microbiomes. Current Biology *30*, R1131–R1137. https://doi.org/10.1016/j.cub.2020.08.005.

3. Zhou, Y., Wang, H., Sun, J., Wicaksono, W.A., Liu, C., He, Y., Qin, Y., Berg, G., Li, L., Lin, H., et al. (2025). Phenazines contribute to microbiome dynamics by targeting topoisomerase IV. Nat Microbiol *10*, 2396–2411. https://doi.org/10.1038/s41564-025-02118-0.

4. Dar, D., Thomashow, L.S., Weller, D.M., and Newman, D.K. (2020). Global landscape of phenazine biosynthesis and biodegradation reveals species-specific colonization patterns in agricultural soils and crop microbiomes. eLife *9*, e59726. https://doi.org/10.7554/eLife.59726.

5. Menezes-Blackburn, D., Giles, C., Darch, T., George, T.S., Blackwell, M., Stutter, M., Shand, C., Lumsdon, D., Cooper, P., Wendler, R., et al. (2018). Opportunities for mobilizing recalcitrant phosphorus from agricultural soils: a review. Plant Soil *427*, 5–16. https://doi.org/10.1007/s11104-017-3362-2.

6. McRose, D.L., and Newman, D.K. (2021). Redox-active antibiotics enhance phosphorus bioavailability. Science *371*, 1033–1037. https://doi.org/10.1126/science.abd1515.

7. Cox, C.D. (1986). Role of pyocyanin in the acquisition of iron from transferrin. Infection and Immunity *52*, 263–270. https://doi.org/10.1128/iai.52.1.263-270.1986.

603 8. Hernandez, M.E., Kappler, A., and Newman, D.K. (2004). Phenazines and other redox-active
604 antibiotics promote microbial mineral reduction. Appl Environ Microbiol *70*, 921–928.
605 https://doi.org/10.1128/AEM.70.2.921-928.2004.

606 9. Wang, Y., Wilks, J.C., Danhorn, T., Ramos, I., Croal, L., and Newman, D.K. (2011). Phenazine-1-
607 Carboxylic Acid Promotes Bacterial Biofilm Development via Ferrous Iron Acquisition. Journal of
608 Bacteriology *193*, 3606–3617. https://doi.org/10.1128/jb.00396-11.

609 10. LeTourneau, M.K., Marshall, M.J., Grant, M., Freeze, P.M., Strawn, D.G., Lai, B., Dohnalkova,
610 A.C., Harsh, J.B., Weller, D.M., and Thomashow, L.S. (2019). Phenazine-1-Carboxylic Acid-
611 Producing Bacteria Enhance the Reactivity of Iron Minerals in Dryland and Irrigated Wheat
612 Rhizospheres. Environ. Sci. Technol. *53*, 14273–14284. https://doi.org/10.1021/acs.est.9b03962.

613 11. Price-Whelan, A., Dietrich, L.E.P., and Newman, D.K. (2006). Rethinking "secondary" metabolism:
614 physiological roles for phenazine antibiotics. Nat Chem Biol *2*, 71–78.
615 https://doi.org/10.1038/nchembio764.

616 12. Meirelles, L.A., and Newman, D.K. (2018). Both toxic and beneficial effects of pyocyanin contribute
617 to the lifecycle of Pseudomonas aeruginosa. Molecular Microbiology *110*, 995–1010.
618 https://doi.org/10.1111/mmi.14132.

619 13. Perry, E.K., and Newman, D.K. (2022). Prevalence and Correlates of Phenazine Resistance in
620 Culturable Bacteria from a Dryland Wheat Field. Applied and Environmental Microbiology *88*,
621 e02320-21. https://doi.org/10.1128/aem.02320-21.

622 14. Thomashow, L.S., and Weller, D.M. (1988). Role of a phenazine antibiotic from Pseudomonas
623 fluorescens in biological control of Gaeumannomyces graminis var. tritici. J Bacteriol *170*, 3499–
624 3508. https://doi.org/10.1128/jb.170.8.3499-3508.1988.

625 15. Chin-A-Woeng, T.F.C., Bloemberg, G.V., and Lugtenberg, B.J.J. (2003). Phenazines and their role in
626 biocontrol by Pseudomonas bacteria. New Phytologist *157*, 503–523. https://doi.org/10.1046/j.1469-
627 8137.2003.00686.x.

628 16. LeTourneau, M.K., Marshall, M.J., Cliff, J.B., Bonsall, R.F., Dohnalkova, A.C., Mavrodi, D.V.,
629 Devi, S.I., Mavrodi, O.V., Harsh, J.B., Weller, D.M., et al. (2018). Phenazine-1-carboxylic acid and
630 soil moisture influence biofilm development and turnover of rhizobacterial biomass on wheat root
631 surfaces. Environmental Microbiology *20*, 2178–2194. https://doi.org/10.1111/1462-2920.14244.

632 17. Fuqua, W.C., Winans, S.C., and Greenberg, E.P. (1994). Quorum sensing in bacteria: the LuxR-LuxI
633 family of cell density-responsive transcriptional regulators. J Bacteriol *176*, 269–275.
634 https://doi.org/10.1128/jb.176.2.269-275.1994.

635 18. Venturi, V. (2006). Regulation of quorum sensing in Pseudomonas. FEMS Microbiol Rev *30*, 274–
636 291. https://doi.org/10.1111/j.1574-6976.2005.00012.x.

637 19. Miller, M.B., and Bassler, B.L. (2001). Quorum Sensing in Bacteria. Annual Review of
638 Microbiology *55*, 165–199. https://doi.org/10.1146/annurev.micro.55.1.165.

639 20. Waters, C.M., and Bassler, B.L. (2005). QUORUM SENSING: Cell-to-Cell Communication in
640 Bacteria. Annual Review of Cell and Developmental Biology *21*, 319–346.
641 https://doi.org/10.1146/annurev.cellbio.21.012704.131001.

642 21. Parsek, M.R., and Greenberg, E.P. (2005). Sociomicrobiology: the connections between quorum
643 sensing and biofilms. Trends Microbiol *13*, 27–33. https://doi.org/10.1016/j.tim.2004.11.007.

644 22. Papenfort, K., and Bassler, B.L. (2016). Quorum sensing signal–response systems in Gram-negative
645 bacteria. Nat Rev Microbiol *14*, 576–588. https://doi.org/10.1038/nrmicro.2016.89.

646 23. Abisado, R.G., Benomar, S., Klaus, J.R., Dandekar, A.A., and Chandler, J.R. (2018). Bacterial
647 Quorum Sensing and Microbial Community Interactions. mBio *9*, e02331-17.
648 https://doi.org/10.1128/mBio.02331-17.

649 24. Whiteley, M., Diggle, S.P., and Greenberg, E.P. (2017). Bacterial quorum sensing: the progress and
650 promise of an emerging research area. Nature *551*, 313–320. https://doi.org/10.1038/nature24624.

651 25. Mukherjee, S., and Bassler, B.L. (2019). Bacterial quorum sensing in complex and dynamically
652 changing environments. Nat Rev Microbiol *17*, 371–382. https://doi.org/10.1038/s41579-019-0186-5.

653 26. Raynaud, X., and Nunan, N. (2014). Spatial Ecology of Bacteria at the Microscale in Soil. PLOS
654 ONE *9*, e87217. https://doi.org/10.1371/journal.pone.0087217.

655 27. Wang, G., and Or, D. (2010). Aqueous films limit bacterial cell motility and colony expansion on
656 partially saturated rough surfaces. Environmental Microbiology *12*, 1363–1373.
657 https://doi.org/10.1111/j.1462-2920.2010.02180.x.

658 28. Tecon, R., and Or, D. (2017). Biophysical processes supporting the diversity of microbial life in soil.
659 FEMS Microbiol Rev *41*, 599–623. https://doi.org/10.1093/femsre/fux039.

660 29. Mavrodi, D.V., Mavrodi, O.V., Parejko, J.A., Bonsall, R.F., Kwak, Y.-S., Paulitz, T.C., Thomashow,
661 L.S., and Weller, D.M. (2012). Accumulation of the Antibiotic Phenazine-1-Carboxylic Acid in the
662 Rhizosphere of Dryland Cereals. Applied and Environmental Microbiology *78*, 804–812.
663 https://doi.org/10.1128/AEM.06784-11.

664 30. Mavrodi, D.V., Mavrodi, O.V., Elbourne, L.D.H., Tetu, S., Bonsall, R.F., Parejko, J., Yang, M.,
665 Paulsen, I.T., Weller, D.M., and Thomashow, L.S. (2018). Long-Term Irrigation Affects the
666 Dynamics and Activity of the Wheat Rhizosphere Microbiome. Front. Plant Sci. *9*.
667 https://doi.org/10.3389/fpls.2018.00345.

668 31. Schuhegger, R., Ihring, A., Gantner, S., Bahnweg, G., Knappe, C., Vogg, G., Hutzler, P., Schmid, M.,
669 Van Breusegem, F., Eberl, L., et al. (2006). Induction of systemic resistance in tomato by N-acyl-L-
670 homoserine lactone-producing rhizosphere bacteria. Plant Cell Environ *29*, 909–918.
671 https://doi.org/10.1111/j.1365-3040.2005.01471.x.

672 32. DeAngelis, K.M., Firestone, M.K., and Lindow, S.E. (2007). Sensitive Whole-Cell Biosensor
673 Suitable for Detecting a Variety of N-Acyl Homoserine Lactones in Intact Rhizosphere Microbial
674 Communities. Appl Environ Microbiol *73*, 3724–3727. https://doi.org/10.1128/AEM.02187-06.

675 33. DeAngelis, K.M., Lindow, S.E., and Firestone, M.K. (2008). Bacterial quorum sensing and nitrogen
676 cycling in rhizosphere soil. FEMS Microbiol Ecol *66*, 197–207. https://doi.org/10.1111/j.1574-
677 6941.2008.00550.x.

678 34. Redfield, R.J. (2002). Is quorum sensing a side effect of diffusion sensing? Trends in Microbiology
679 *10*, 365–370. https://doi.org/10.1016/S0966-842X(02)02400-9.

680 35. Hense, B.A., Kuttler, C., Müller, J., Rothballer, M., Hartmann, A., and Kreft, J.-U. (2007). Does
681 efficiency sensing unify diffusion and quorum sensing? Nat Rev Microbiol *5*, 230–239.
682 https://doi.org/10.1038/nrmicro1600.

683 36. Platt, T.G., and Fuqua, C. (2010). What's in a name? The semantics of quorum sensing. Trends
684 Microbiol *18*, 383–387. https://doi.org/10.1016/j.tim.2010.05.003.

685 37. West, S.A., Winzer, K., Gardner, A., and Diggle, S.P. (2012). Quorum sensing and the confusion
686 about diffusion. Trends in Microbiology *20*, 586–594. https://doi.org/10.1016/j.tim.2012.09.004.

687 38. Boedicker, J.Q., Vincent, M.E., and Ismagilov, R.F. (2009). Microfluidic Confinement of Single
688 Cells of Bacteria in Small Volumes Initiates High-Density Behavior of Quorum Sensing and Growth
689 and Reveals Its Variability. Angewandte Chemie International Edition *48*, 5908–5911.
690 https://doi.org/10.1002/anie.200901550.

691 39. Darch, S.E., Simoska, O., Fitzpatrick, M., Barraza, J.P., Stevenson, K.J., Bonnecaze, R.T., Shear,
692 J.B., and Whiteley, M. (2018). Spatial determinants of quorum signaling in a Pseudomonas
693 aeruginosa infection model. Proceedings of the National Academy of Sciences *115*, 4779–4784.
694 https://doi.org/10.1073/pnas.1719317115.

695 40. Stewart, P.S. (2003). Diffusion in Biofilms. Journal of Bacteriology *185*, 1485–1491.
696 https://doi.org/10.1128/jb.185.5.1485-1491.2003.

697 41. Parsek, M.R., and Greenberg, E.P. (2005). Sociomicrobiology: the connections between quorum
698 sensing and biofilms. Trends Microbiol *13*, 27–33. https://doi.org/10.1016/j.tim.2004.11.007.

699 42. Kim, M.K., Ingremeau, F., Zhao, A., Bassler, B.L., and Stone, H.A. (2016). Local and global
700 consequences of flow on bacterial quorum sensing. Nat Microbiol *1*, 15005.
701 https://doi.org/10.1038/nmicrobiol.2015.5.

702 43. Hense, B.A., Müller, J., Kuttler, C., and Hartmann, A. (2012). Spatial Heterogeneity of Autoinducer
703 Regulation Systems. Sensors *12*, 4156–4171. https://doi.org/10.3390/s120404156.

704 44. Thomashow, L.S., and Weller, D.M. (1988). Role of a phenazine antibiotic from Pseudomonas
705 fluorescens in biological control of Gaeumannomyces graminis var. tritici. J Bacteriol *170*, 3499–
706 3508. https://doi.org/10.1128/jb.170.8.3499-3508.1988.

707 45. Mavrodi, D.V., Ksenzenko, V.N., Bonsall, R.F., Cook, R.J., Boronin, A.M., and Thomashow, L.S.
708 (1998). A Seven-Gene Locus for Synthesis of Phenazine-1-Carboxylic Acid by Pseudomonas
709 fluorescens 2-79. J Bacteriol *180*, 2541–2548.

710 46. Khan, S.R., Mavrodi, D.V., Jog, G.J., Suga, H., Thomashow, L.S., and Farrand, S.K. (2005).
711 Activation of the phz Operon of Pseudomonas fluorescens 2-79 Requires the LuxR Homolog PhzR,
712 N-(3-OH-Hexanoyl)-l-Homoserine Lactone Produced by the LuxI Homolog PhzI, and a cis-Acting
713 phz Box. J Bacteriol *187*, 6517–6527. https://doi.org/10.1128/JB.187.18.6517-6527.2005.

714 47. Khan, S.R., Herman, J., Krank, J., Serkova, N.J., Churchill, M.E.A., Suga, H., and Farrand, S.K.
715 (2007). N-(3-Hydroxyhexanoyl)-l-Homoserine Lactone Is the Biologically Relevant Quormone That
716 Regulates the phz Operon of Pseudomonas chlororaphis Strain 30-84. Applied and Environmental
717 Microbiology *73*, 7443–7455. https://doi.org/10.1128/AEM.01354-07.

718 48. Zhang, O., Alcalde, R.E., Zhou, H., Yin, S., Newman, D.K., and Yang, C. (2024). Investigating 3D
719 microbial community dynamics of the rhizosphere using quantitative phase and fluorescence
720 microscopy. Proceedings of the National Academy of Sciences *121*, e2403122121.
721 https://doi.org/10.1073/pnas.2403122121.

722 49. Holford, I.C.R. (1997). Soil phosphorus: its measurement, and its uptake by plants. Soil Res. *35*,
723 227–240. https://doi.org/10.1071/s96047.

724 50. Hinsinger, P. (2001). Bioavailability of soil inorganic P in the rhizosphere as affected by root-induced
725 chemical changes: a review. Plant and Soil *237*, 173–195. https://doi.org/10.1023/A:1013351617532.

726 51. Ducousso-Détrez, A., Fontaine, J., Lounès-Hadj Sahraoui, A., and Hijri, M. (2022). Diversity of
727 Phosphate Chemical Forms in Soils and Their Contributions on Soil Microbial Community Structure
728 Changes. Microorganisms *10*, 609. https://doi.org/10.3390/microorganisms10030609.

729 52. Whooley, M.A., and McLoughlin, A.J. (1982). The regulation of pyocyanin production in
730 Pseudomonas aeruginosa. European J. Appl. Microbiol. Biotechnol. *15*, 161–166.
731 https://doi.org/10.1007/BF00511241.

732 53. Jensen, V., Löns, D., Zaoui, C., Bredenbruch, F., Meissner, A., Dieterich, G., Münch, R., and
733 Häussler, S. (2006). RhlR Expression in Pseudomonas aeruginosa Is Modulated by the Pseudomonas
734 Quinolone Signal via PhoB-Dependent and -Independent Pathways. JB *188*, 8601–8606.
735 https://doi.org/10.1128/JB.01378-06.

736 54. Oglesby, A.G., Farrow, J.M., Lee, J.-H., Tomaras, A.P., Greenberg, E.P., Pesci, E.C., and Vasil, M.L.
737 (2008). The influence of iron on Pseudomonas aeruginosa physiology: a regulatory link between iron
738 and quorum sensing. J Biol Chem *283*, 15558–15567. https://doi.org/10.1074/jbc.m707840200.

739 55. Lee, J., Wu, J., Deng, Y., Wang, J., Wang, C., Wang, J., Chang, C., Dong, Y., Williams, P., and
740 Zhang, L.-H. (2013). A cell-cell communication signal integrates quorum sensing and stress
741 response. Nat Chem Biol *9*, 339–343. https://doi.org/10.1038/nchembio.1225.

742 56. Nguyen, A.T., Jones, J.W., Ruge, M.A., Kane, M.A., and Oglesby-Sherrouse, A.G. (2015). Iron
743 Depletion Enhances Production of Antimicrobials by Pseudomonas aeruginosa. J Bacteriol *197*,
744 2265–2275. https://doi.org/10.1128/JB.00072-15.

745 57. Welsh, M.A., and Blackwell, H.E. (2016). Chemical Genetics Reveals Environment-Specific Roles
746 for Quorum Sensing Circuits in *Pseudomonas aeruginosa*. Cell Chemical Biology *23*, 361–369.
747 https://doi.org/10.1016/j.chembiol.2016.01.006.

748 58. Meng, X., Ahator, S.D., and Zhang, L.-H. (2020). Molecular Mechanisms of Phosphate Stress
749 Activation of Pseudomonas aeruginosa Quorum Sensing Systems. mSphere *5*,
750 10.1128/msphere.00119-20. https://doi.org/10.1128/msphere.00119-20.

751 59. Monds, R.D., Newell, P.D., Schwartzman, J.A., and O'Toole, G.A. (2006). Conservation of the Pho
752 regulon in Pseudomonas fluorescens Pf0-1. Appl Environ Microbiol *72*, 1910–1924.
753 https://doi.org/10.1128/AEM.72.3.1910-1924.2006.

754 60. Hsieh, Y.-J., and Wanner, B.L. (2010). Global Regulation by the Seven-component Pi Signaling
755 System. Curr Opin Microbiol *13*, 198–203. https://doi.org/10.1016/j.mib.2010.01.014.

61. Santos-Beneit, F. (2015). The Pho regulon: a huge regulatory network in bacteria. Front. Microbiol. *6*. https://doi.org/10.3389/fmicb.2015.00402.

62. Goldberg, S., and Sposito, G. (1984). A Chemical Model of Phosphate Adsorption by Soils: I. Reference Oxide Minerals. Soil Science Soc of Amer J *48*, 772–778. https://doi.org/10.2136/sssaj1984.03615995004800040015x.

63. Dzombak, D.A., and Morel, F. (1990). Surface complexation modeling: hydrous ferric oxide (Wiley).

64. Boyd, V., Yoon, H., Zhang, C., Oostrom, M., Hess, N., Fouke, B., Valocchi, A.J., and Werth, C.J. (2014). Influence of Mg2+ on CaCO3 precipitation during subsurface reactive transport in a homogeneous silicon-etched pore network. Geochimica et Cosmochimica Acta *135*, 321–335. https://doi.org/10.1016/j.gca.2014.03.018.

65. van Delden, C., Comte, R., and Bally, A.M. (2001). Stringent Response Activates Quorum Sensing and Modulates Cell Density-Dependent Gene Expression inPseudomonas aeruginosa. Journal of Bacteriology *183*, 5376–5384. https://doi.org/10.1128/jb.183.18.5376-5384.2001.

66. Diggle, S.P., Winzer, K., Chhabra, S.R., Worrall, K.E., Cámara, M., and Williams, P. (2003). The Pseudomonas aeruginosa quinolone signal molecule overcomes the cell density-dependency of the quorum sensing hierarchy, regulates rhl-dependent genes at the onset of stationary phase and can be produced in the absence of LasR. Molecular Microbiology *50*, 29–43. https://doi.org/10.1046/j.1365-2958.2003.03672.x.

67. Dubern, J.-F., Halliday, N., Cámara, M., Winzer, K., Barrett, D.A., Hardie, K.R., and Williams, P. (2023). Growth rate and nutrient limitation as key drivers of extracellular quorum sensing signal molecule accumulation in Pseudomonas aeruginosa. Microbiology *169*, 001316. https://doi.org/10.1099/mic.0.001316.

68. W. G. Sunda, N. M. Price, and F. M. M. Morel (2005). Algal culturing techniques R. A. Andersen, ed. (Elsevier/Academic Press).

69. Choi, K.-H., and Schweizer, H.P. (2006). mini-Tn 7 insertion in bacteria with single att Tn 7 sites: example Pseudomonas aeruginosa. Nat Protoc *1*, 153–161. https://doi.org/10.1038/nprot.2006.24.